

Provided for non-commercial research and education use.
Not for reproduction, distribution or commercial use.



This article appeared in a journal published by Elsevier. The attached copy is furnished to the author for internal non-commercial research and education use, including for instruction at the authors institution and sharing with colleagues.

Other uses, including reproduction and distribution, or selling or licensing copies, or posting to personal, institutional or third party websites are prohibited.

In most cases authors are permitted to post their version of the article (e.g. in Word or Tex form) to their personal website or institutional repository. Authors requiring further information regarding Elsevier's archiving and manuscript policies are encouraged to visit:

<http://www.elsevier.com/copyright>



A study on electric properties for pulse laser annealing of ITO film after wet etching

C.J. Lee ^a, H.K. Lin ^{b,*}, C.H. Li ^c, L.X. Chen ^d, C.C. Lee ^d, C.W. Wu ^d, J.C. Huang ^a

^a Department of Materials and Optoelectronic Science, Center for Nanoscience and Nanotechnology, National Sun Yat-Sen University, Kaohsiung 804, Taiwan, ROC

^b Graduate Institute of Materials Engineering, National Pingtung University of Science and Technology, 1, Shuefu Road, Neipu, Pingtung 912, Taiwan, ROC

^c Laser Application Technology Center/Industrial Technology Research Institute South (ITRI South), 8, Gongyan Rd., Liujia Shiang, Tainan 734, Taiwan, ROC

^d Display Technology Center/Industrial Technology Research Institute, Hsinchu, Taiwan, ROC

ARTICLE INFO

Article history:

Received 8 August 2011

Received in revised form 4 September 2012

Accepted 4 September 2012

Available online 12 September 2012

Keywords:

Indium tin oxide
Nanosecond pulse laser
Annealing
Crystallization
Wet etching

ABSTRACT

The electric properties of ITO thin film after UV or IR laser annealing and wet etching was analyzed via grazing incidence in-plane X-ray diffraction, scanning electron microscopy, X-ray photoelectron spectra and residual stress measurement. The laser annealing process readily induced microcracks or quasi-microcracks on the ITO thin film due to the residual tension stress of crystalline phase transformation between irradiated and non-irradiated areas, and these defects then became the preferred sites for a higher etching rate, resulting in discontinuities in the ITO thin film after the wet etching process. The discontinuities in the residual ITO thin film obstruct carrier transmission and further result in electric failure.

Crown Copyright © 2012 Published by Elsevier B.V. All rights reserved.

1. Introduction

Transparent conductive oxides (TCOs) with the characteristics of high transparency and low resistance are popular materials for use in the current transparent conductors. Indium–Tin oxide (ITO) is a major material in products such as flat panel displays (FPD), organic light-emitting devices and solar cells [1–3]. The patterning of ITO thin film is an important, complex and necessary procedure in some applications of active or light-emitting devices. In the traditional approach, using photolithography, the processes include photoresist coating, baking, photoresist developing, and material etching, and although this is a mature technology, it is also complex and requires a considerable amount of time and expense. Developing an easier and faster process to pattern an ITO thin film has thus been a topic of some interest in the recent two decades, and direct laser writing is one promising approach.

Laser patterning can follow one of two approaches. One is direct laser ablation [4–12], which uses long- (nanosecond) [4–6,10–12] or ultrafast- pulses (picosecond and femtosecond) [7–9], and the influence of various parameters, including the different wavelengths, irradiated energies, repetition rates, and scanning speeds on the ablation of ITO thin films has been extensively studied. However, the laser ablation process has the potential weaknesses of leaving residual ITO materials or damaging the substrate, especially for devices that are fabricated directly onto the substrate, meaning that this approach has a number of limitations. The other method uses a combination of laser annealing

and wet etching [13–17], and utilizes laser writing and lower levels of irradiated energy to achieve a local and patterning transformation from an amorphous ITO phase to crystalline ITO phase. It then exploits the characteristic of the lower etching rate for the crystalline ITO phase than the amorphous ITO one to preserve the crystalline ITO film, thus achieving the goal of patterning. The combination of phase transformation and wet etching, which has the advantage of less substrate damage than the laser ablation, presents a potential processing route for patterning ITO thin films, especially the processing of active devices. In addition to this advantage, the patterning and annealing processes are integrated into one work to improve the conductivity and transparency of ITO films, and this will reduce the working time compared to processes like furnace annealing and photolithography.

To date, there are few cases in the literature that examine the combination of laser annealing and wet etching processes, except for some works that utilize femtosecond or excimer lasers [13,15–17]. The main drawback of such a combined approach is that the ITO thin films produced after laser annealing and wet etching processes are more likely to suffer from electric failure or microcracking [6,14]. Moreover, the relationship between this combined method process and electric failure for ITO thin films still remains unclear. Therefore, the current study aimed to investigate the relationship between laser annealing and wet etching and electric failure for two different nanosecond lasers of 1064 and 355 nm.

2. Experimental method

ITO thin films with a thickness of ~100 nm were deposited on glass substrate (AGC G2 size 0.7 mm glass) at ambient temperature by a RF

* Corresponding author. Tel.: +886 8 7703202 7568; fax: +886 8 7740552.
E-mail address: hsuankai@msn.com (H.K. Lin).

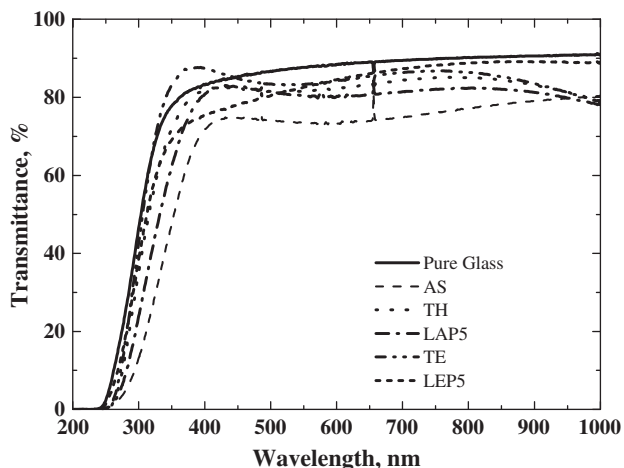


Fig. 1. Optical transmittance spectra for the various processing ITO specimens.

magnetron sputtering system (UNI-4500) using the In_2O_3 (90 wt.%): SnO_2 (10 wt.%) target, termed as AS. The working power was operated at 3 kW and the sputtering time was 29 s. These gas flows of Ar, H_2 and O_2 were 22, 5 and 6 sccm, respectively. The laser experiments were conducted using a UV laser (Coherent AVIA 355–7000) with a wavelength of 355 nm, a repetition rate of 40–120 kHz, and a pulse duration of < 35 ns, and an IR laser (SPI SP-20P) with a wavelength of 1064 nm, repetition rate of 25–500 kHz, and pulse duration of > 10 ns. The specimens then underwent the following various laser annealing processes: (1) 355 nm laser, repetition rate of 40 kHz, irradiation power of 57 mW, scan speed of 50 mm/s, scan pitch of 5 μm , (2) 355 nm laser, repetition rate of 40 kHz, irradiation power of 38 mW, scan speed of 100 mm/s, scan pitch of 5 μm , and (3) 1064 nm laser, repetition rate of 500 kHz, irradiation power of 622 mW, scan speed of 100 mm/s, scan pitch of 25 μm . These three laser annealing processes took place in a square of 10×10 mm with a spot size of 42 μm , and are named (1) LAP5, (2) LAP3 and (3) LAR6, respectively. In order to check the differences between furnace annealing and laser annealing, general furnace annealing of 200 °C for 1 h was also conducted, termed as TH. After annealing, these specimens were immersed into a 0.1 N oxalic acid etchant at 40 °C for 2 min, and named (1) LEP5, (2) LEP3, (3) LER6 and (4) TE, respectively.

The crystalline, optical and electrical properties of these specimens before and after etching were measured by grazing incidence in-plane X-ray diffraction (Bruker D8 Advance, GIXRD), UV–VIS–IR spectrophotometry (N&K analyzer 1280), and the four-point probe technique. The morphology and components ratio of films were examined by scanning electron microscopy (JEOL-6330 SEM). The chemical compound information for oxygen and indium was examined using a JPS-9010MX X-ray Photoelectron Spectroscopy (XPS) with monochromatic $\text{Al K}\alpha$ X-ray source. A pass energy of 30 eV was used and the scanning method was a step of 0.1 eV with 300 μs duration. The samples were scanned for 5 times. Before scanning samples, they were cleaned with Ar^+ ion polish for 30 s. Before identifying the chemical bonding information for oxygen and indium, their energy spectra were corrected with carbon bonding (285 eV). Then, the background was subtracted from the corrected spectra with Shirley method. The oxygen and indium bonding were identified from the final spectra. The residual stress of ITO thin films

Table 1
Measurement results of the four-point probe for the various ITO specimens. (Unit: Ω/\square).

	AS-ITO	TH-ITO	LAP5-ITO	LAP3-ITO	LAR6-ITO
Before etching	110	20	50	80	25
After etching	–	20	Over flow	Over flow	Over flow

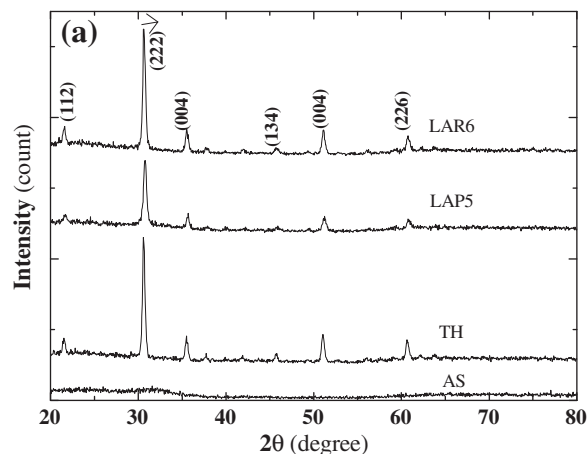


Fig. 2. The GIXRD results of various ITO specimens before (a) and after (b) wet etching.

after furnace and laser annealing was measured by an experimental method using GIXRD based on the conventional $\sin^2\psi$ method [18].

3. Results and discussions

Fig. 1 and Table 1 present the optical transmittance and conductivity, respectively, for the AS specimen, furnace annealing and laser annealing ITO specimens. The results show that the transmittance of the AS specimen improved from 74% to 81% at a wavelength of 550 nm, regardless of whether the furnace annealing or laser annealing process was used. In addition, the sheet resistivity of $110 \Omega/\square$ of the AS specimen was lowered after the annealing processes. Comparing the two different processes, the enhancement in conductivity seen with laser annealing ($80\text{--}25 \Omega/\square$) was less than that seen with furnace annealing ($\sim 20 \Omega/\square$). No matter which process is used, appropriate annealing can improve the conductivity of as-deposited ITO thin films at ambient temperature based on enhanced mobility and reduced scattering of the carriers [19,20].

Fig. 2 shows the GIXRD results for the various ITO specimens before and after wet etching. The as-deposited ITO thin film (AS) is an amorphous structure, with no diffracted peaks, just a relatively

Table 2
The carrier density and mobility for the various ITO specimens obtained by Hall measurement.

	AS-ITO	TH-ITO	LAP3-ITO
Mobility (cm^2/Vs)	$1.30\text{E}+01$	$2.28\text{E}+01$	$6.43\text{E}+00$
Carrier density (cm^{-3})	$4.37\text{E}+20$	$1.32\text{E}+21$	$9.50\text{E}+20$

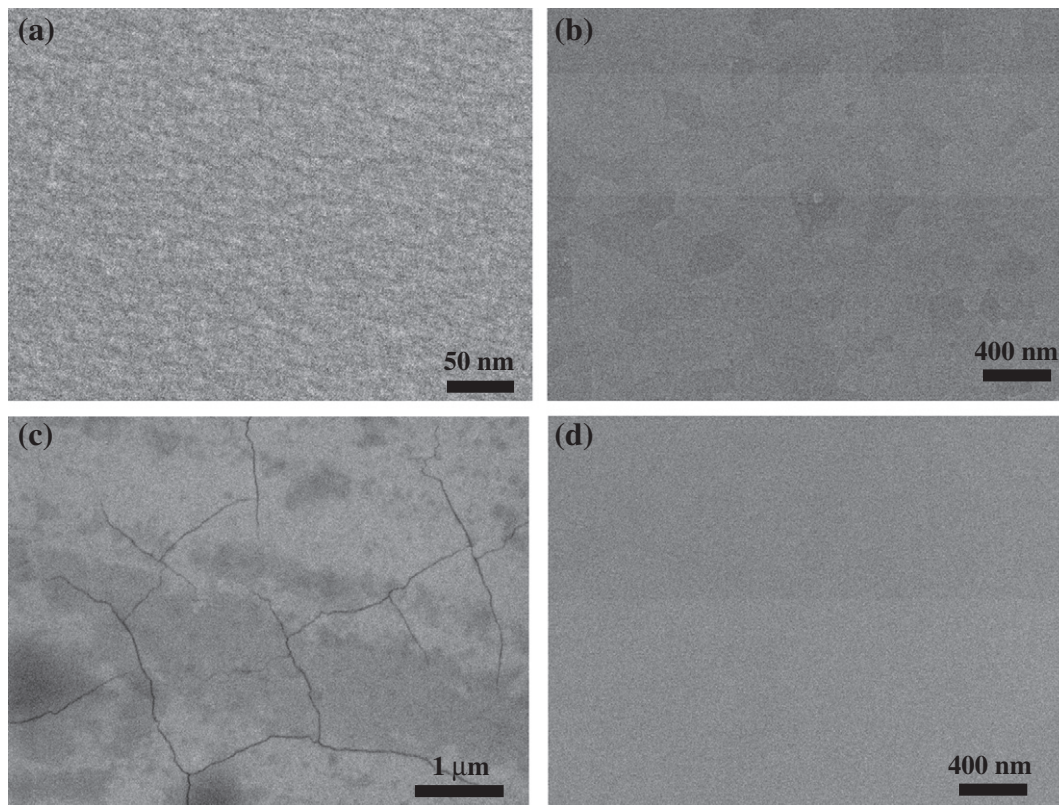


Fig. 3. SEM photographs showing the morphology of the various processing ITO thin film before wet etching: (a) AS, (b) TH, (c) LAP5 and (d) LAR6.

broaden hump at 2θ of $30\text{--}35^\circ$, as shown in Fig. 2(a). After furnace or laser annealing, all the specimens show polycrystalline diffraction peaks, for example, (222), (004) or (226). These results correspond

to a longer mean-free path for carriers in the crystalline structure than in the amorphous structure due to this phase transformation. Therefore, this enhanced mobility of carriers can effectively improve

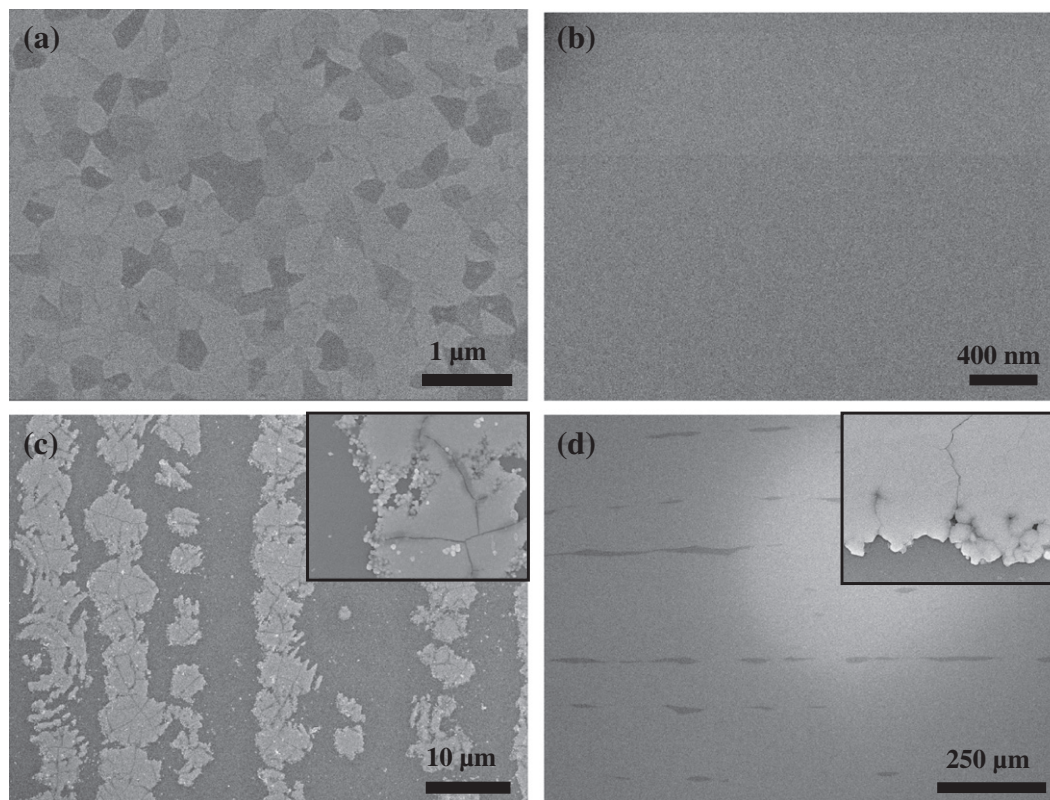


Fig. 4. SEM photographs showing the morphology of the various processing ITO thin film after wet etching: (a) TE, (b) LEP, (c) LEP3 and (d) LER6.

the conductivity of the ITO thin film (Table 2). After wet etching, the furnace annealed ITO specimen (TE) still kept the polycrystalline structure, but the LEP5-ITO specimen, which was annealed by higher UV laser energy, lost the diffracted peaks, showing the amorphous structure of the glass substrate with a broadening hump at 2θ of 22–28°. These results imply that the ITO thin film was completely etched. When the UV laser with lower energy (LEP3) and IR laser annealing (LER6) were used, the ITO thin films could maintain the polycrystalline structure, but the intensity of diffracted peaks for the LEP3 specimen was weakened. These GIXRD results suggest that the presence or absence of ITO thin film after wet etching does not seem to be linked with conductivity, and this will be explored and analyzed in more detail below.

The morphology of the as-deposited ITO film was very smooth, with no apparent or column grains. However, cluster particles of 20–30 nm in diameter were clearly seen at higher magnification, as shown in Fig. 3(a), meaning the size of the ITO molecules from nucleation and growth to coalescence was about 20–30 nm during the deposition process. After the furnace annealing, the grain morphology of ~300 nm in diameter could be observed, as shown in Fig. 3(b), consistent with the GIXRD results. After higher UV laser energy annealing (LAP5), the ITO thin film showed many microcracks, and the interspace between these was about 1–3 μm , as shown in Fig. 3(c). It should be noted that the ITO thin film was smooth and clear without microcracks after IR laser annealing (LAR6), as shown in Fig. 3(d). Fig. 4 shows the morphology of various ITO thin films after wet etching. The TE specimen shows more apparent grain boundaries and a grain size of 200–300 nm, as shown in Fig. 4(a). However, the LEP6 specimen does not show the grain morphology

of the ITO thin film, implying that ITO film was almost etched completely, as shown in Fig. 4(b). In contrast, the lower UV laser energy specimen (LEP3) shows the residual ITO film with a band shape, and this band-shaped ITO film exhibits many microcracks, as shown in Fig. 4(c). The smooth and clear ITO film of LAR6 shows many etched grooves and displays microcracks in the residual ITO film after wet etching, as shown in Fig. 4(d).

In the XPS spectra, the In3d spectra show In3d_{5/2} and In3d_{3/2} peaks at 444.5 and 452.1 eV, respectively, for the AS, TH, LAP5 and TE specimens, as shown in Fig. 5(a), consistent with measurement results in other studies [21–25], but the LEP5 specimen does not have any In3d peaks. The O1s spectra of the AS, TH, LAP5 and TE specimens could be roughly fitted by two main peaks of 530 and 531.5 eV, which correspond to the energy of In–O bonding and In(OH)₃ or InOOH bonding, respectively [21,26]. In contrast, the main peak of the O1s spectrum for LEP5 is shifted to 532.5 eV, which corresponds to the Si–O bonding energy. Integrating the foregoing GIXRD and SEM results, it can be confirmed that the ITO film of the LEP5 specimen was etched completely and the LAP3 and LAR6 specimens had less and more ITO film, respectively, after wet etching. In other words, the etching rate of the higher UV laser energy annealing is the fastest, followed by the lower UV laser energy annealing, with the IR laser annealing being slowest.

The high angle (226) peak at $2\theta_0$ of 60.7° was used to measure the residual stress of ITO film with an incident angle, γ , of 1 by grazing incident X-ray diffraction geometry [18]. Fixing the constant α angle, $\alpha = \theta_0 - \gamma$, and tilting the different Ψ angle can get the variation of $(d - d_0)/d_0$ as a function of $\cos^2\alpha \sin^2\Psi$, where d_0 is the initial lattice space, as shown in Fig. 6. The slope, fitted by linear regression method, of TH and LAP5 specimens is 0.00038 and 0.00562, respectively. The residual stress, σ , can be determined from the slope equaling function of $((1 + \nu)/E)\sigma$, where ν and E are the Poisson ratio (~0.33) and Young's modulus (~160 GPa), respectively. Therefore, the residual stress of ~700 MPa for the LAP5 specimen is significantly higher than that of TH specimen (~45 MPa).

4. Discussion

The main goal of annealing is to transform the amorphous ITO film with a short-range order and loose atomic structure into a polycrystalline one with long-range order and a denser structure at elevated temperatures, as the polycrystalline structure can reduce the scattering of carriers and improve conductivity. This phase transformation from an amorphous to a crystalline structure will deplete the extra free volume in the unit space and cause shrinkage in unit volume. It is well known that laser annealing is a local and rapid process, confined to the irradiated area. This irradiated area will experience the phase transformation from an amorphous structure to a polycrystalline one, and this will also induce a tension stress between the irradiated and non-irradiated areas due to the shrinkage in volume during crystalline transformation. The accumulation of tension stress will further cause the emergence of microcracks, and a schematic illustration of this is shown in Fig. 7(a) and (b).

The $\text{C}_2\text{O}_4^{2-}$ ion is the main ion used to etch ITO films during wet etching with oxalic acid, and the etching rate is dominated by an interface-controlled mechanism, not a diffusion-controlled one [27]. The LAP5 specimen with a large amount of microcracks seems to create an extra reaction interface, compared with the TH specimen. Thus, after the same condition of wet etching, the ITO film of the LAP5 specimen was completely etched or removed to result in the insulation of the LEP5 specimen. It is noted that the LAR6 specimen without microcracks also has the characteristic of non-conductivity after wet etching. Yavas and Takai [11] examined the ablation characteristics of a nanosecond laser with a wavelength from 262 nm to 1047 nm for ITO films deposited on glass substrate. The glass substrate not absorbing the IR or visible laser will easily cause lateral heat

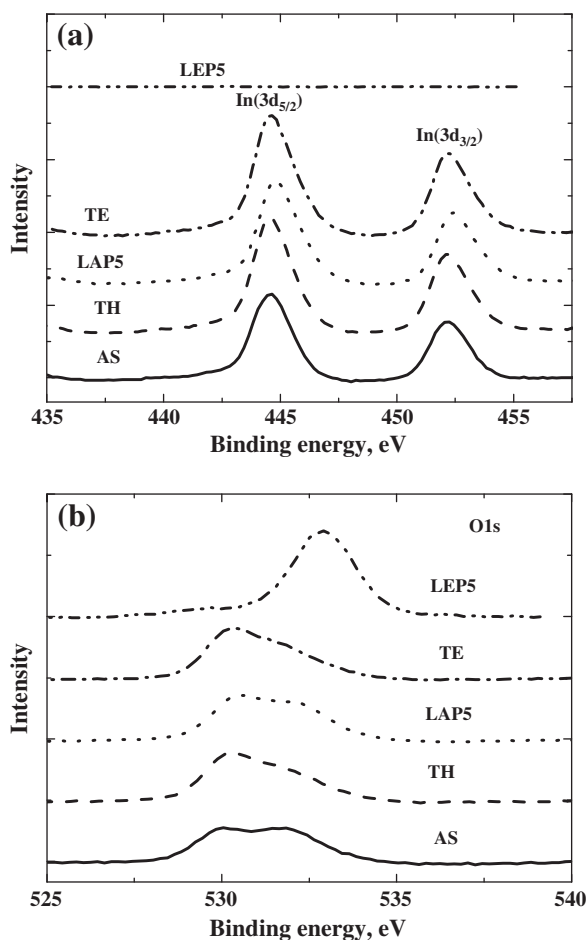


Fig. 5. XPS spectra for the various processing ITO thin film: (a) In3d spectra and (b) O1s spectra.

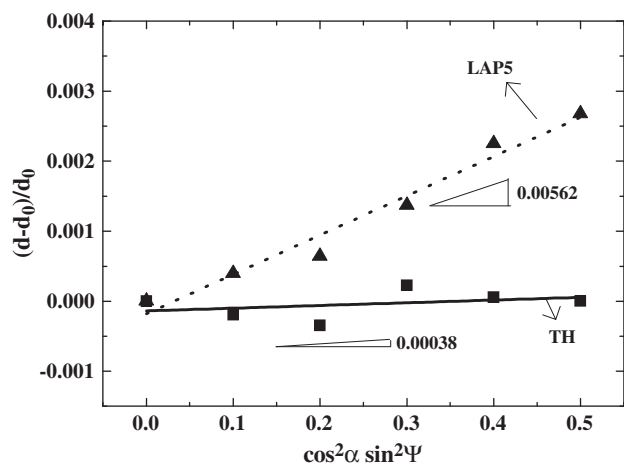


Fig. 6. The $(d - d_0)/d_0$ vs. $\cos^2\alpha \sin^2\Psi$ plot of TH and LAP5 specimens.

conduction due to the poor thermal conductivity, and thus the thermal influence area is greater than the irradiated area, which will further reduce the thermal shock compared to the process with a UV laser. Although the thermal shock of IR laser annealing is insufficient to reach the threshold of inducing microcracks, the boundaries of the thermal influence zone still accumulate high tension stress. These high tension stress boundaries can be regarded as quasi-microcracks, which will be the preferred sites of the higher etching rate, as shown in Fig. 7(c). This can be directly proven from the many etched grooves and microcracks in the residual ITO film after wet etching, as shown in Fig. 4(d). After wet etching, these residual ITO films form discontinuous films and contain large amounts of microcracks that can obstruct the transmission of carriers. Therefore, after wet etching these laser annealed ITO films had the characteristic of non-conductivity.

From the comparison of the residual amount of ITO films and microcrack density, it can be seen that LER6 specimens had the more ITO films and fewer microcracks than the LEP3 ones, as shown in Fig. 4(c) and (d), and it can be inferred that the thermal shock of an IR laser to ITO films is lower than that of a UV laser with lower

energy. Moreover, the lower repetition rate of the pulsed laser will more readily cause a severer thermal shock due to the longer time interval between the emitted lasers than the thermal transmission time of ITO films. This is one reason why the current IR laser can perform lower thermal shock than a UV laser owing to the higher repetition rate, in addition to the different substrate absorption for different laser wavelengths. Considering all factors for reducing thermal shock, such as irradiation energy, substrate absorption, repetition rate, scanning speed, and so on, it is suggested that future research investigates the influences of laser parameters with a higher repetition rate, lower irradiated energy and scanning speed in order to achieve laser annealing without microcracks after wet etching. The authors of the current work have already demonstrated that ITO thin films still have the characteristic of conductivity after laser annealing and wet etching, and the systematical results will be published later.

5. Conclusions

ITO thin film deposited on glass substrate readily suffers from electric failure after laser annealing and wet etching, compared with the outcome of furnace annealing and wet etching. Based on the results of XPS, SEM and residual stress measurements, the laser annealing process induces microcracks or quasi-microcracks on ITO thin films, and these defects then become the preferred sites for a higher etching rate, resulting in discontinuities in the films after wet etching. These discontinuities would obstruct the carrier transmission and result in electric failure. These processing defects originate from the residual tension stress of the crystalline phase transformation between irradiated and non-irradiated areas. Decreasing the thermal shock during laser annealing is suggested in order to reduce these processing defects.

Acknowledgment

The authors gratefully acknowledge the financial support from the National Science Council of Taiwan, R.O.C., under grants NSC 101-2218-E-020-001, NSC 101-2120-M-110-007, NSC 99-2811-E-110-006 and NSC 99-2818-E-110-002. The authors would like to acknowledge

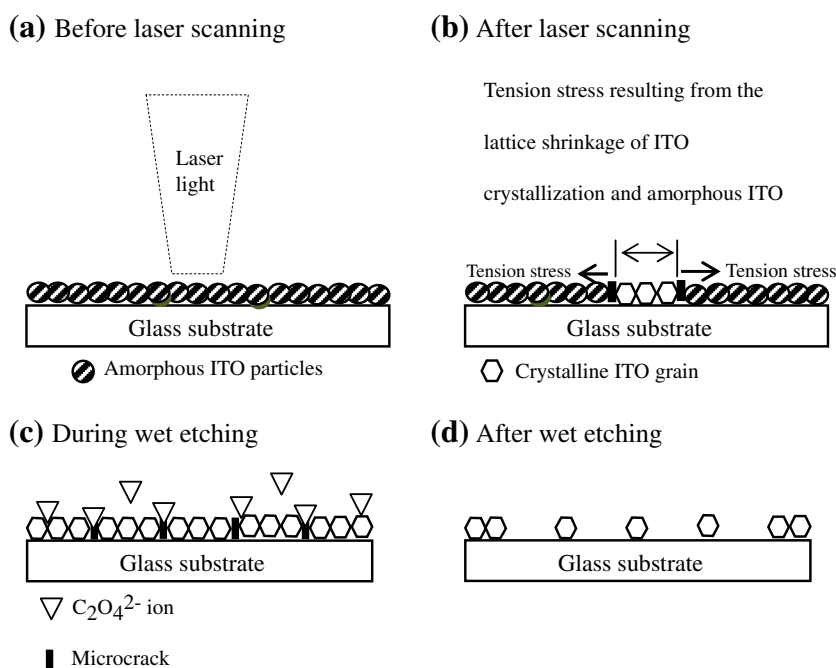


Fig. 7. Schematic illustration of laser annealing inducing the electrical failure for ITO thin film after wet etching.

Prof. D.L. Cheng and Mr. K.H. Chang in the Department of Computer and Communication, SHU-TE University for their assistance in the Hall experiment.

References

- [1] C. Guillen, J. Herrero, *Sol. Energy Mater. Sol. Cells* 92 (8) (2008) 938.
- [2] A. Kloppel, B. Meyer, J. Trube, *Thin Solid Films* 392 (2) (2001) 311.
- [3] H. Kim, C.M. Gilmore, A. Pique, J.S. Horwitz, H. Mattoussi, H. Murata, Z.H. Kafafi, D.B. Chrisey, *J. Appl. Phys.* 86 (11) (1999) 6451.
- [4] Z.H. Li, E.S. Cho, S.J. Kwon, *Appl. Surf. Sci.* 255 (24) (2009) 9843.
- [5] M.F. Chen, W.T. Hsiao, Y.S. Ho, S.F. Tseng, Y.P. Chen, *Thin Solid Films* 518 (4) (2009) 1072.
- [6] G. Legeay, X. Castel, R. Benzerga, J. Pinel, *Phys. Status Solidi C* 5 (10) (2008) 3248.
- [7] G. Raciukaitis, M. Brikas, M. Gedvilas, G. Darcianovas, *J. Laser Micro/Nanoeng.* 2 (1) (2007) 1.
- [8] H.W. Choi, D.F. Farson, J. Bovatsek, A. Arai, D. Ashkenasi, *Appl. Optics* 46 (23) (2007) 5792.
- [9] M. Park, B.H. Chon, H.S. Kim, S.C. Jeoung, D. Kim, J.I. Lee, H.Y. Chu, H.R. Kim, *Opt. Lasers Eng.* 44 (2) (2006) 138.
- [10] C. Molpeceres, S. Lauzurica, J.L. Ocana, J.J. Gandia, L. Urbina, J. Carabe, *J. Micromech. Microeng.* 15 (6) (2005) 1271.
- [11] O. Yavas, M. Takai, *J. Appl. Phys.* 85 (8) (1999) 4207.
- [12] O. Yavas, M. Takai, *Appl. Phys. Lett.* 73 (18) (1998) 2558.
- [13] C.W. Cheng, C.Y. Lin, W.C. Shen, Y.J. Lee, J.S. Chen, *Thin Solid Films* 518 (2010) 7138.
- [14] C.W. Cheng, J.S. Chen, H.H. Chen, *Mater. Manuf. Process.* 25 (7) (2010) 684.
- [15] J. Chae, L. Jang, K. Jain, *Mater. Lett.* 64 (8) (2010) 948.
- [16] C.W. Cheng, W.C. Shen, Y.J. Lee, J.S. Chen, C.W. Chien, *J. Laser Micro/Nanoeng.* 4 (3) (2009) 234.
- [17] H. Hosono, M. Kurita, H. Kawazoe, *Jpn. J. Appl. Phys. Part 2 - Lett.* 37/10A (1998) L1119.
- [18] C.H. Ma, J.H. Huang, H. Chen, *Thin Solid Films* 418 (2) (2002) 73.
- [19] H. Morikawa, M. Fujita, *Thin Solid Films* 359 (2000) 61.
- [20] T.J. Coutts, D.L. Young, X.N. Li, *MRS Bull.* 25 (8) (2000) 58.
- [21] J.H. Wi, J.C. Woo, D.S. Um, J. Kim, C.I. Kim, *Thin Solid Films* 518 (22) (2010) 6228.
- [22] R.X. Wang, C.D. Belling, S. Fung, A.B. Djuricic, C.C. Ling, S. Li, *J. Appl. Phys.* 97 (3) (2005).
- [23] C.J. Huang, Y.K. Su, S.L. Wu, *Mater. Chem. Phys.* 84 (1) (2004) 146.
- [24] F.R. Zhu, C.H.A. Huan, K.R. Zhang, A.T.S. Wee, *Thin Solid Films* 359 (2) (2000) 244.
- [25] K. Utsumi, O. Matsunaga, T. Takahata, *Thin Solid Films* 334 (1–2) (1998) 30.
- [26] M.J. Chuang, H.F. Huang, C.H. Wen, A.K. Chu, *Thin Solid Films* 518 (8) (2010) 2290.
- [27] T.H. Tsai, Y.F. Wu, *Microelectron. Eng.* 83 (3) (2006) 536.